

Article

Behavior of Sliding Angle as Function of Temperature Difference between Droplet and Superhydrophobic Coating for Aircraft Ice Protection Systems

Mitsugu Hasegawa ¹, Haruka Endo ², Katsuaki Morita ³, Hiroataka Sakaue ¹ and Shigeo Kimura ^{4,*}

- ¹ Department of Aerospace and Mechanical Engineering, University of Notre Dame, Notre Dame, IN 46556, USA; mhasegaw@nd.edu (M.H.); hsakaue@nd.edu (H.S.)
- ² Meteorological Research Institute for Technology, Bunkyo, Tokyo 113-0033, Japan; skyeycorundum@gmail.com
- ³ Next Generation Aeronautical Innovation Hub Center, Japan Aerospace Exploration Agency, Mitaka, Tokyo 181-0015, Japan; morita.katsuaki@jaxa.jp
- ⁴ Department of Mechanical Engineering, Kanagawa Institute of Technology, Atsugi 243-0292, Kanagawa, Japan
- * Correspondence: skimura@me.kanagawa-it.ac.jp; Tel.: +81-46-291-3132

Abstract: A hybrid anti-/de-icing system combining a superhydrophobic coating and an electrothermal heater is an area of active research for aircraft icing prevention. The heater increases the temperature of the interaction surface between impinging droplets and an aircraft surface. One scientific question that has not been studied in great detail is whether the temperatures of the droplet and the surface or the temperature difference between the two dominate the anti-/de-icing performance. Herein, this scientific question is experimentally studied based on the mobility of a water droplet over a superhydrophobic coating. The mobility is characterized by the sliding angle between the droplet and the coating surface. It was found that the temperature difference between the droplet and the coating surface has a higher impact on the sliding angle than their individual temperatures.

Keywords: aircraft icing; anti-/de-icing; superhydrophobic coating; sliding angle; temperature



Citation: Hasegawa, M.; Endo, H.; Morita, K.; Sakaue, H.; Kimura, S. Behavior of Sliding Angle as Function of Temperature Difference between Droplet and Superhydrophobic Coating for Aircraft Ice Protection Systems. *Aerospace* **2021**, *8*, 219. <https://doi.org/10.3390/aerospace8080219>

Academic Editor: Doni Daniel

Received: 30 June 2021
Accepted: 5 August 2021
Published: 8 August 2021

Publisher's Note: MDPI stays neutral with regard to jurisdictional claims in published maps and institutional affiliations.



Copyright: © 2021 by the authors. Licensee MDPI, Basel, Switzerland. This article is an open access article distributed under the terms and conditions of the Creative Commons Attribution (CC BY) license (<https://creativecommons.org/licenses/by/4.0/>).

1. Introduction

Aircraft icing is a hazardous event for many aircrafts, because it impacts aerodynamic performance leading to potentially fatal accidents [1–5]. An evaporative system for anti-/de-icing has conventionally been used to prevent aircraft icing. However, energy efficiency using bleed air has been an issue, as these systems are energetically and economically expensive [6–9]. A hybrid anti-/de-icing system combining a superhydrophobic coating with an electrothermal heater has recently been proposed to reduce energy consumption [10–13]. Ice accretion over the leading edge of a wing is melted by the heater. The melted water droplets can be easily removed from the superhydrophobic coating surface by gravity or an aerodynamic force, because the droplet's mobility over the surface is enhanced by the hydrophobicity of the coating [14–22]. To enable a hybrid anti-/de-icing system, the superhydrophobic coating surface must promote this ease of droplet removal for different temperature conditions.

A droplet's mobility over a superhydrophobic coating is evaluated by measuring the sliding angle of the water droplet placed on the coating surface [23–26]. Here, the scientific question arises whether the temperatures of the droplet and the surface or the temperature difference between the two dominates the droplet's mobility. The temperatures of the droplet and the superhydrophobic coating surface have impacts on the surface tension and viscosity of the droplet, as well as the wetting mode of the superhydrophobic coating surface, which all influence the sliding angle [27–30]. However, the fundamental behavior of the sliding angle, where the temperature of the droplet is different from that of the

superhydrophobic coating surface, has not been well studied for icing conditions where subfreezing temperatures are given.

The present study experimentally investigates the effects of both the temperatures of the droplet and the surface and the temperature difference between the two on a droplet's mobility. Sliding angle measurements between the droplet and the coating surface were performed to characterize the mobility of the superhydrophobic coating surface based on a dynamic evaluation method [31]. The temperature difference between the droplets and the superhydrophobic coating surface was given to identify the influence of the temperature and the temperature difference on the sliding angle. Droplet and surface temperatures ranging from $-5\text{ }^{\circ}\text{C}$ to $25\text{ }^{\circ}\text{C}$ were studied to mimic conditions where anti-/de-icing is performed using a heated superhydrophobic coating surface under icing conditions. The ambient temperature was fixed at $-10\text{ }^{\circ}\text{C}$. The combination of temperatures simulated the possible combinations of heated melted/cooled water and heated/cooled superhydrophobic coating surfaces under icing conditions.

2. Method

The dynamic evaluation method describes how quickly a droplet moves over a coating surface. The method determines the minimum tilt angle required to move the droplet. The amount of energy required to move the droplet is measured by applying a force. The force is applied to the droplet by tilting the coating surface as shown in Figure 1. The component of gravity parallel to the coating surface drives the droplet. The angle, when gravity overcomes the adhesion force, is obtained by the following Equation [24,31]:

$$mg \sin \beta = \gamma_L W (\cos \theta_R - \cos \theta_A), \quad (1)$$

where m is the mass of the droplet, g is gravity, β is the sliding angle, γ_L is the surface tension of water, and W is the contact length of the droplet; θ_A and θ_R are advancing and receding angles, respectively. A lower β indicates a better anti-/de-icing performance, as it means a lower force is necessary to remove the droplet [31].

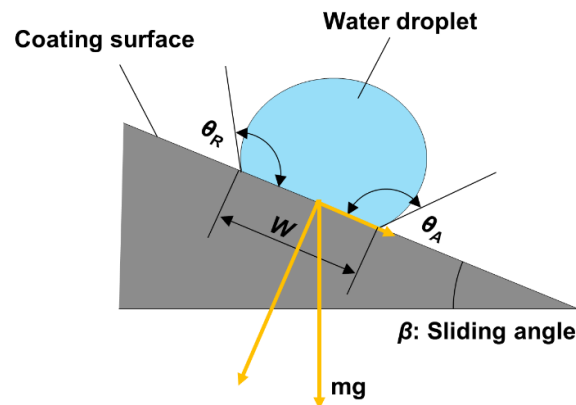


Figure 1. Schematic description of a water droplet on a tilted coating surface.

3. Experimental Setup

Figure 2 shows the schematic of the sliding angle measurement setup. The measurements of the sliding angles were performed using a computer-controlled contact angle meter (KYOWA, DM-701, Saitama, Japan) in a temperature-controlled chamber with 750 mm in width, 460 mm in height, and 440 mm in depth (Espec, WU-200, Osaka, Japan). A superhydrophobic coating plate was installed at the stage of the sliding angle meter with a temperature-controlled heater mat. A superhydrophobic coating, HIREC 450 (NTT A.T. Corp., Tokyo, Japan) for anti-/de-icing, was applied to an aluminum plate of A5052 by spraying. Ten microliters of water droplets were dispensed on the temperature-controlled superhydrophobic coating plate using a temperature-controlled syringe. The temperature

of the water droplet, T_d , was measured using a thermocouple embedded at the syringe tip. The temperature of the superhydrophobic coating surface, T_c , was defined using a thermocouple embedded between the coated plate and the heater mat.

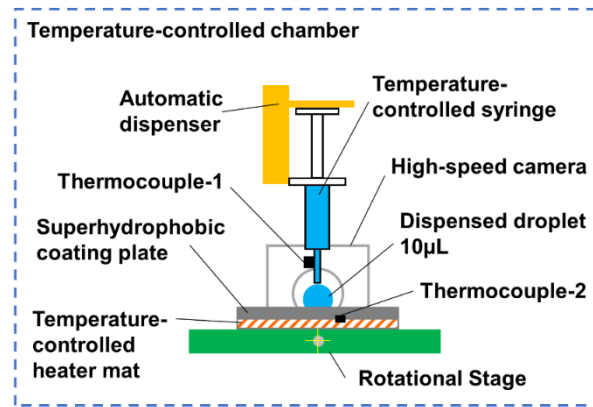


Figure 2. Schematic description of the sliding angle measurement setup. Thermocouple-1 measures the temperature of the water droplet, T_d . Thermocouple-2 measures the temperature that defines the temperature of the superhydrophobic coating surface, T_c .

The temperatures of the droplet and the superhydrophobic coating surface during the experiments were $-5\text{ }^{\circ}\text{C}$, $5\text{ }^{\circ}\text{C}$, and $25\text{ }^{\circ}\text{C}$. The temperature difference, ΔT , between the water droplet, T_d , and the superhydrophobic coating surface, T_c , varied between $-30\text{ }^{\circ}\text{C}$ and $30\text{ }^{\circ}\text{C}$ to study conditions where anti-/de-icing was performed using a superhydrophobic coating surface with a heater under icing conditions. The ambient temperature of the chamber, T_a , was fixed at $-10\text{ }^{\circ}\text{C} \pm 0.3\text{ }^{\circ}\text{C}$ to simulate icing conditions where supercooled droplet impingement occurs. The temperatures conditions during the experiments are summarized in Table 1.

Table 1. Temperatures of the water droplet and the superhydrophobic coating surface and the temperature difference between the two.

Temperature Difference, $\Delta T = T_d - T_c$ ($^{\circ}\text{C}$)	Temperature of Water Droplet, T_d ($^{\circ}\text{C}$)		
	-5	5	25
Temperature of the superhydrophobic coating surface, T_c ($^{\circ}\text{C}$)	-5	10	30
	5	0	20
	25	-30	0

The sliding angles were determined using image acquisition software and a high-speed camera. The superhydrophobic coating plate was angled to induce the roll-off of the droplet, after the droplet was dispensed. The images of the droplet were taken while the plate was rotated, until the droplet began to roll on the plate. The sliding angle measurements were taken, when droplets moved for 0.5 mm . The sliding angles were measured using Famas analysis software. The frame rate for the camera was 500 frames per second. The measurements for the contact length and the sliding angle were performed 5 times to reduce uncertainty.

4. Results

Figure 3 shows the sliding angles for different temperatures, where the temperature of the droplet, T_d , was equal to that of the superhydrophobic coating surface, T_c . The sliding angles were 8° , 7° , and 8° for the temperatures of $-5\text{ }^{\circ}\text{C}$, $5\text{ }^{\circ}\text{C}$, and $25\text{ }^{\circ}\text{C}$, respectively. The sliding angles were almost constant and were less than 10° for each temperature. A sliding angle of less than 10° demonstrates the comparative mobility of the present superhydrophobic coating compared with those reported in similar studies using superhydrophobic coatings [31,32]. It was found that temperature variation did

not affect the sliding angle when the temperature of the droplet was equal to that of the superhydrophobic coating surface.

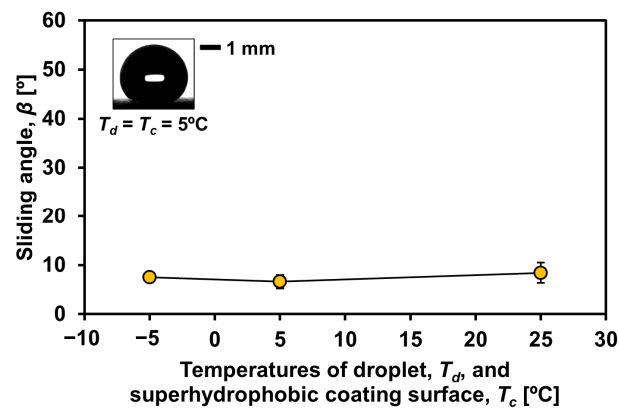


Figure 3. Sliding angle as a function of temperature where there is no temperature difference between the water droplet and the superhydrophobic coating surface. Error bars represent the standard deviations of repeated experiments.

Figure 4 shows the sliding angles for various temperature differences, ΔT , between the temperature of the droplet, T_d , and temperature of the superhydrophobic coating surface, T_c . As shown, sliding angles were almost constant and less than 10° for $\Delta T \leq 0$. As previously mentioned, the sliding angle of less than 10° means the comparative mobility of the superhydrophobic coating, regardless of the temperature difference. However, sliding angles significantly increased, as ΔT increased for $\Delta T > 0$. Sliding angles were 17° , 41° , and 49° for $\Delta T = 10^\circ\text{C}$, 20°C , and 30°C , respectively. The increase in sliding angle indicated the increasing adhesion force between the droplet and the superhydrophobic coating surface. The superhydrophobic coating surface showed reduced water repellency and became more adhesive with respect to water. It was found that temperature differences did impact the sliding angle, when the temperature of the droplet, T_d , was higher than that of the superhydrophobic coating surface, T_c .

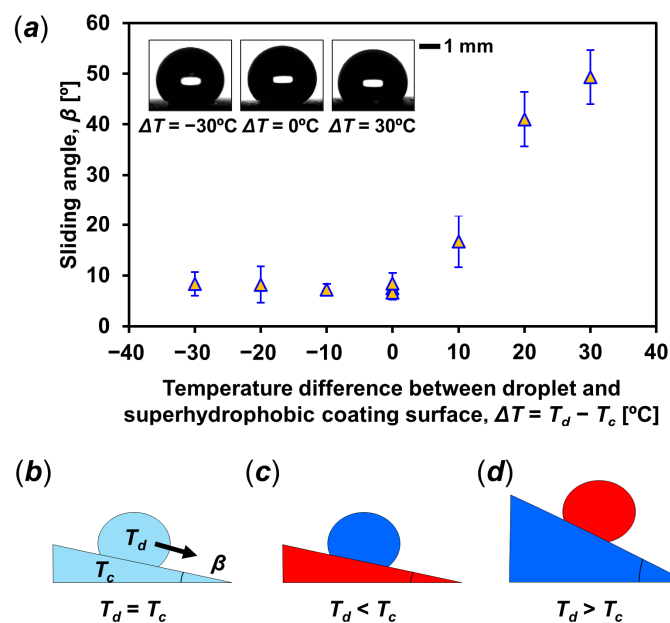


Figure 4. (a) Sliding angle as a function of temperature difference, ΔT , between the water droplet temperature, T_d , and the superhydrophobic coating surface temperature, T_c . Error bars represent the standard deviations of the repeated experiments. (b–d) Classification of sliding angles corresponding to temperature differences.

5. Discussion

The increasing sliding angle can be caused by the condensation of water vapor due to the temperature difference between the droplet and the superhydrophobic coating surface. The water vapor from the droplet surface condenses on the coating surface. If the roughness of the coating surface is partially/fully filled by the cluster of the condensed water vapor, the mobility of the superhydrophobic coating is degraded, which causes an increase in sliding angle due to the change from the Cassie-Baxter wetting mode to the Wenzel wetting mode [29,30,33–36]. As long as the temperature of the droplet is higher than that of the superhydrophobic coating surface, i.e., $\Delta T > 0$, the water vapor from the droplet can condense on the coating surface. In addition, a greater temperature difference drives the water vaporization and condensation, enhancing the change of wetting mode from the Cassie-Baxter model to the fully Wenzel model. In fact, only for $\Delta T > 0$, where the temperature of the droplet was higher than that of the superhydrophobic coating surface, was a significant increase in sliding angle observed, as shown in Figure 4. The significant increase in the sliding angles compared with the cases for $\Delta T \leq 0$ implied the change of wetting mode from the Cassie-Baxter mode with lower adhesion to the Wenzel mode with higher adhesion [25]. Furthermore, a greater temperature difference resulted in a higher sliding angle, as shown in Figure 4.

The evaporation rate of the droplet, dm/dt , depends on the temperature difference and is described as follows, if convective and conductive heat transfer between the droplet and the air is neglected [37]:

$$\frac{dm}{dt} = 4\pi r D_V \rho_a \frac{P_{sat,d} - P_{sat,a}}{P_a} \frac{M_V}{M_a}, \quad (2)$$

where r is the droplet radius, D_V is the diffusion coefficient of the water vapor in the air, ρ_a is the air density, P_a is the air pressure, $P_{sat,d}$ and $P_{sat,a}$ are the saturated vapor pressure at the temperature of the droplet surface and the air around the droplet, respectively, and M_V and M_a are the molecular weights of the water vapor and the air, respectively. The saturated vapor pressure is a function of temperature, so it can be expected that a greater temperature difference leads to water vaporization, increasing the moisture over the colder superhydrophobic coating surface.

The condensation rate of the water vapor was also considered. The rate of condensation growth, dr/dt , can be approximated as follows [38–40]:

$$\frac{dr}{dt} \approx h_i \left(\frac{T_{sat} - T_c}{\rho_L H_f} \right), \quad (3)$$

where h_i is the interfacial heat transfer coefficient [38], T_{sat} is the saturated air temperature, i.e., the temperature of the saturated vapor within roughness, H_f is the latent heat of vaporization, and ρ_L is the water density. Here, the saturated air temperature was defined as $T_{sat} = (T_d - T_c)/2$, so the rate of condensation growth depended on the temperature difference. Equation (3) indicates that a larger temperature difference enhances the condensation over the colder superhydrophobic coating surface.

The sliding angle of superhydrophobic coatings is influenced by the temperatures of droplets and superhydrophobic coating surfaces [31,32]. However, the temperature difference between the droplet and superhydrophobic coating surface is also a considerable parameter to evaluate the sliding angle of the superhydrophobic coating when ΔT of > 0 is given as a potential condition. In fact, the change in the temperatures of the droplet and the superhydrophobic coating surface did not show a significant impact on the sliding angles measured, as shown in Figure 3, where there was no temperature difference between the droplet and the superhydrophobic coating surface. In contrast, an increasing temperature difference significantly impacted the sliding angles for $\Delta T > 0$, where droplet cooling occurred, as shown in Figure 4.

6. Conclusions

The influences of the temperatures of a water droplet and a superhydrophobic coating surface and the temperature difference between the two on a sliding angle were investigated to identify whether the temperatures or the temperature difference dominate the droplet's mobility. The temperature difference was given by setting the temperatures of a droplet and a superhydrophobic coating surface to $-5\text{ }^{\circ}\text{C}$, $5\text{ }^{\circ}\text{C}$, and $25\text{ }^{\circ}\text{C}$. It was concluded that the temperature difference has a more critical impact on the droplet's mobility than the temperatures themselves. If the droplet temperature was equal to the superhydrophobic coating surface temperature, i.e., $\Delta T = 0$, a change in the temperatures did not significantly impact the sliding angle. Sliding angles remained nearly constant and were less than 10° for $\Delta T = 0$. If the droplet temperature was lower than the superhydrophobic coating surface temperature, i.e., $\Delta T < 0$, the sliding angle also remained less than 10° , regardless of the size of the temperature difference. However, if the temperature of the droplet was higher than that of the superhydrophobic coating surface, i.e., $\Delta T > 0$, temperature differences ΔT of $10\text{ }^{\circ}\text{C}$, $20\text{ }^{\circ}\text{C}$, and $30\text{ }^{\circ}\text{C}$ had impacts on the sliding angle with observed sliding angles of 17° , 41° , and 49° , respectively. The temperature difference had a higher impact than the temperatures of the droplet and the coating surface. For successful aircraft icing prevention, the temperature difference should be as low as possible during droplets' travel. A significant temperature difference can fail to remove melted droplets from a superhydrophobic coating surface, causing an ice accretion. In other words, excessively heated melted droplets adhere to a colder superhydrophobic coating surface during the droplets' travel, causing secondary icing. An equipped heater must properly warm the superhydrophobic coating surface to keep temperature difference low, until the droplets are removed from the surface.

Author Contributions: Conceptualization, H.S. and S.K.; methodology, K.M., H.S., and S.K.; validation, H.E., K.M., and H.S.; formal analysis, M.H., H.E., and K.M.; investigation, H.E. and K.M.; resources, H.S. and S.K.; data curation, M.H. and H.E.; writing—original draft preparation, M.H. and H.E.; writing—review and editing, H.S.; supervision, K.M., H.S., and S.K.; project administration, K.M. and H.S.; funding acquisition, H.S. and S.K. All authors have read and agreed to the published version of the manuscript.

Funding: This research received no external funding.

Institutional Review Board Statement: Not applicable.

Informed Consent Statement: Not applicable.

Data Availability Statement: The data presented in this study are available on request from the corresponding author, upon reasonable request.

Conflicts of Interest: The authors declare no conflict of interest.

References

1. Gent, R.W.; Dart, N.P.; Cansdale, J.T. Aircraft icing. *Philos. Trans. R. Soc. A Math. Phys. Eng. Sci.* **2000**, *358*, 2873–2911. [[CrossRef](#)]
2. Bragg, M.B. Aircraft aerodynamic effects due to large droplet ice accretions. In *Proceedings of the 34th Aerospace Sciences Meeting and Exhibit*; American Institute of Aeronautics and Astronautics Inc.: Reston, VA, USA, 1996.
3. Bragg, M.B.; Perkins, W.R.; Sorter, N.B.; Basar, T.; Voulgaris, P.G.; Gurbacki, H.M.; Melody, J.W.; Mccray, S.A. An interdisciplinary approach to inflight aircraft icing safety. In *Proceedings of the 36th AIAA Aerospace Sciences Meeting and Exhibit*; American Institute of Aeronautics and Astronautics Inc.: Reston, VA, USA, 1998.
4. Addy, H.E. *Ice Accretions and Icing Effects for Modern Airfoils*; NASA/TP-2000-210031 (also DOT/FAA/AR-99/89); NASA: Cleveland, OH, USA, 2000.
5. Cao, Y.; Tan, W.; Wu, Z. Aircraft icing: An ongoing threat to aviation safety. *Aerosp. Sci. Technol.* **2018**, *75*, 353–385. [[CrossRef](#)]
6. FAA. *Pilot Guid: Flight In Icing Conditions*; Advisory Circular AC 91-74B; Federal Aviation Administration: Washington, DC, USA, 2015.
7. Meier, O.; Scholz, D. *A Handbook Method for the Estimation of Power Requirements for Electrical De-Icing Systems*; DLRK: Hamburg, Germany, 2010.
8. Yeoman, K. *Efficiency of a Bleed Air Powered Inlet Icing Protective System*; American Institute of Aeronautics and Astronautics: Reston, VA, USA, 1994.

9. Pellissier, M.P.C.; Habashi, W.G.; Pueyo, A. Optimization via FENSAP-ICE of Aircraft Hot-Air Anti-Icing Systems. *J. Aircr.* **2010**, *48*, 265–276. [[CrossRef](#)]
10. Kimura, S.; Yamagishi, Y.; Sakabe, A.; Adachi, T.; Shimanuki, M. A new surface coating for prevention of icing on airfoils. In *Proceedings of the SAE Technical Papers*; SAE International: Warrendale, PA, USA, 2007.
11. Antonini, C.; Innocenti, M.; Horn, T.; Marengo, M.; Amirfazli, A. Understanding the effect of superhydrophobic coatings on energy reduction in anti-icing systems. *Cold Reg. Sci. Technol.* **2011**, *67*, 58–67. [[CrossRef](#)]
12. Morita, K.; Kimura, S.; Sakaue, H. Hybrid system combining ice-phobic coating and electrothermal heating for wing ice protection. *Aerospace* **2020**, *7*, 102. [[CrossRef](#)]
13. Hann, R.; Enache, A.; Nielsen, M.C.; Stovner, B.N.; van Beeck, J.; Johansen, T.A.; Borup, K.T. Experimental heat loads for electrothermal anti-icing and de-icing on uavs. *Aerospace* **2021**, *8*, 83. [[CrossRef](#)]
14. Neinhuis, C.; Barthlott, W. Characterization and distribution of water-repellent, self-cleaning plant surfaces. *Ann. Bot.* **1997**, *79*, 667–677. [[CrossRef](#)]
15. Barthlott, W.; Neinhuis, C. Purity of the sacred lotus, or escape from contamination in biological surfaces. *Planta* **1997**, *202*, 1–8. [[CrossRef](#)]
16. Lafuma, A.; Quéré, D. Superhydrophobic states. *Nat. Mater.* **2003**, *2*, 457–460. [[CrossRef](#)] [[PubMed](#)]
17. Blossey, R. Self-cleaning surfaces—Virtual realities. *Nat. Mater.* **2003**, *2*, 301–306. [[CrossRef](#)]
18. Fürstner, R.; Barthlott, W.; Neinhuis, C.; Walzel, P. Wetting and self-cleaning properties of artificial superhydrophobic surfaces. *Langmuir* **2005**, *21*, 956–961. [[CrossRef](#)] [[PubMed](#)]
19. Milne, A.J.B.; Amirfazli, A. Drop Shedding by Shear Flow for Hydrophilic to Superhydrophobic Surfaces. *Langmuir* **2009**, *25*, 14155–14164. [[CrossRef](#)] [[PubMed](#)]
20. Mandal, D.K.; Criscione, A.; Tropea, C.; Amirfazli, A. Shedding of Water Drops from a Surface under Icing Conditions. *Langmuir* **2015**, *31*, 9340–9347. [[CrossRef](#)]
21. Roisman, I.V.; Criscione, A.; Tropea, C.; Mandal, D.K.; Amirfazli, A. Dislodging a sessile drop by a high-Reynolds-number shear flow at subfreezing temperatures. *Phys. Rev. E Stat. Nonlinear Soft Matter Phys.* **2015**, *92*, 023007. [[CrossRef](#)]
22. Villeneuve, E.; Brassard, J.-D.; Volat, C. Effect of Various Surface Coatings on De-Icing/Anti-Icing Fluids Aerodynamic and Endurance Time Performances. *Aerospace* **2019**, *6*, 114. [[CrossRef](#)]
23. Furmidge, C.G.L. Studies at phase interfaces. I. The sliding of liquid drops on solid surfaces and a theory for spray retention. *J. Colloid Sci.* **1962**, *17*, 309–324. [[CrossRef](#)]
24. Pierce, E.; Carmona, F.J.; Amirfazli, A. Understanding of sliding and contact angle results in tilted plate experiments. *Colloids Surf. A Physicochem. Eng. Asp.* **2008**, *323*, 73–82. [[CrossRef](#)]
25. Milne, A.J.B.; Elliott, J.A.W.; Zabeti, P.; Zhou, J.; Amirfazli, A. Model and experimental studies for contact angles of surfactant solutions on rough and smooth hydrophobic surfaces. *Phys. Chem. Chem. Phys.* **2011**, *13*, 16208–16219. [[CrossRef](#)]
26. Wang, Z.; Elimelech, M.; Lin, S. Environmental Applications of Interfacial Materials with Special Wettability. *Environ. Sci. Technol.* **2016**, *50*, 2132–2150. [[CrossRef](#)]
27. Yang, C.; Leong, K.C. Influences of substrate wettability and liquid viscosity on isothermal spreading of liquid droplets on solid surfaces. *Exp. Fluids* **2002**, *33*, 728–731. [[CrossRef](#)]
28. Vargaftik, N.B.; Volkov, B.N.; Voljak, L.D. International Tables of the Surface Tension of Water. *J. Phys. Chem. Ref. Data* **1983**, *12*, 817–820. [[CrossRef](#)]
29. Liu, Y.; Chen, X.; Xin, J.H. Can superhydrophobic surfaces repel hot water? *J. Mater. Chem.* **2009**, *19*, 5602–5611. [[CrossRef](#)]
30. Yu, Z.J.; Yang, J.; Wan, F.; Ge, Q.; Yang, L.L.; Ding, Z.L.; Yang, D.Q.; Sacher, E.; Isimjan, T.T. How to repel hot water from a superhydrophobic surface? *J. Mater. Chem. A* **2014**, *2*, 10639–10646. [[CrossRef](#)]
31. Morita, K.; Sakaue, H. Characterization method of hydrophobic anti-icing coatings. *Rev. Sci. Instrum.* **2015**, *86*, 115108. [[CrossRef](#)] [[PubMed](#)]
32. Morita, K.; Gonzales, J.; Sakaue, H. Effect of PTFE particle size on superhydrophobic coating for supercooled water prevention. *Coatings* **2018**, *8*, 426. [[CrossRef](#)]
33. Wier, K.A.; McCarthy, T.J. Condensation on ultrahydrophobic surfaces and its effect on droplet mobility: Ultrahydrophobic surfaces are not always water repellent. *Langmuir* **2006**, *22*, 2433–2436. [[CrossRef](#)]
34. Dorrer, C.; Rühle, J. Condensation and wetting transitions on microstructured ultrahydrophobic surfaces. *Langmuir* **2007**, *23*, 3820–3824. [[CrossRef](#)]
35. Furuta, T.; Sakai, M.; Isobe, T.; Nakajima, A. Effect of dew condensation on the wettability of rough hydrophobic surfaces coated with two different silanes. *Langmuir* **2010**, *26*, 13305–13309. [[CrossRef](#)]
36. Papadopoulos, P.; Mammen, L.; Deng, X.; Vollmer, D.; Butt, H.J. How superhydrophobicity breaks down. *Proc. Natl. Acad. Sci. USA* **2013**, *110*, 3254–3258. [[CrossRef](#)]
37. Zhu, P.; Chen, R.; Wang, L. Topography-Directed Hot-Water Super-Repellent Surfaces. *Adv. Sci.* **2019**, *6*, 1900798. [[CrossRef](#)]
38. Shiri, S.; Murrizi, A.; Bird, J.C. Trapping a Hot Drop on a Superhydrophobic Surface with Rapid Condensation or Microtexture Melting. *Micromachines* **2018**, *9*, 566. [[CrossRef](#)] [[PubMed](#)]
39. Maa, J.R. Drop size distribution and heat flux of dropwise condensation. *Chem. Eng. J.* **1978**, *16*, 171–176. [[CrossRef](#)]
40. Kim, S.; Kim, K.J. Dropwise Condensation Modeling Suitable for Superhydrophobic Surfaces. *J. Heat Transfer.* **2011**, *133*. [[CrossRef](#)]